

Electric-field-induced ordering and pattern formation in colloidal suspensions

Jae Sung Park and David Saintillan*

Department of Mechanical Science and Engineering, University of Illinois at Urbana-Champaign, Urbana, Illinois 61801, USA

(Received 23 August 2010; revised manuscript received 6 March 2011; published 22 April 2011)

The long-time dynamics and pattern formation in semidilute suspensions of colloidal spheres in a viscous electrolyte under a uniform electric field are investigated using numerical simulations. The rapid chain formation that occurs in the field direction as a result of dipolar interactions is found to be followed by a slow coarsening process by which chains coalesce into hexagonal sheets and eventually rearrange to form mesoscale cellular structures, in qualitative agreement with recent experiments. The morphology and characteristic wavelength of the patterns that emerge at steady state are shown to depend on the suspension's volume fraction, electrode spacing, and field strength, suggesting additional ways of controlling effective suspension properties in practical applications.

DOI: [10.1103/PhysRevE.83.041409](https://doi.org/10.1103/PhysRevE.83.041409)

PACS number(s): 82.70.Dd, 47.54.-r, 47.57.jd, 64.70.pv

I. INTRODUCTION

The ability to manipulate particles at the microscales and nanoscales is critical to many laboratory-on-a-chip devices. To this end, electric fields offer a simple and efficient method for controlling particle motions and are commonly used in a wide range of applications, including directed assembly and nanomanufacturing [1–3], cell and macromolecular sorting [4,5], particle trapping [6,7], among others. Particle motion can be achieved via several types of electrokinetic phenomena, the simplest of which is electrophoresis (EP) [8], or linear motion of a charged particle in an applied electric field. More precise control is sometimes possible using nonlinear electrokinetics, and specifically dielectrophoresis (DEP) [9,10], in which particle motion occurs along field gradients.

When several particles are subject to an external field, electric and hydrodynamic interactions between them may arise and result in relative motions, possibly yielding unexpected or undesirable effects. One such well-documented phenomenon is particle chaining [11,12] that occurs as a result of dipolar interactions between particles, an effect closely related to DEP [13,14]. The resulting chains are also known to interact and sometimes coalesce [15–19] leading to the formation of larger structures [20,21]. The phases that result from these interactions can be highly complex and have yet to be fully characterized [22].

Particle chaining due to dipolar interactions has received much attention in the fields of electrorheology and magnetorheology [20,23–30] since the chains and complex structures that form owing to interactions have a strong impact on the effective viscosity of colloidal suspensions. Specifically, structure formation results in a strong viscosity enhancement that is reversible and controlled by the applied external field. Such electrorheological fluids find a wealth of applications in engineering where they are used, for example, in electromechanical actuators. As their mechanical response is directly related to their microstructure, a good understanding of the structure formation in these systems is of fundamental interest for the design of such devices.

The present study is motivated by two recent and similar sets of experiments by Kumar *et al.* [31] and Agarwal and Yethiraj [32] that investigated the long-time dynamics in dilute to semidilute colloidal suspensions placed in a uniform alternating (ac) electric field between two parallel flat electrodes. Both studies found that the rapid chain formation due to dipolar interactions was followed by a very slow coarsening process, in which large-scale particle-free voids enclosed by particle-rich walls nucleated in the suspensions, leading at steady state to unusual mesoscale cellular patterns previously unobserved in simulations. They speculated that this coarsening and pattern formation were the consequence of chain-chain interactions, although detailed modeling of this phenomenon remains lacking.

In this paper, we present results from large-scale numerical simulations of semidilute suspensions of colloidal spheres subjected to an ac electric field under confinement, with the aim of elucidating this effect [31,32]. Using a detailed algorithm presented in Sec. II, we are able to probe a long range of time scales in suspensions of realistic sizes. Simulation results are presented in Sec. III that reproduce the steady-state cellular structures reported in experiments. Our simulations demonstrate that dipolar interactions are the driving force for this pattern formation, and the effects of the volume fraction, electrode spacing, and electric field strength are analyzed. We show that suspension microstructure can be tuned by adjusting these parameters, yielding a rich variety of phases including random distributions, isolated chains, hexagonal sheets, columnar structures, and ordered cell patterns. Our conclusions are presented in Sec. IV.

II. MODEL AND METHODS

We consider a suspension of N identical spherical particles of radius a , suspended in a viscous electrolyte (with permittivity ϵ and viscosity η) between two parallel flat electrodes. The suspension is doubly periodic in the x - y plane of the electrodes, but nonperiodic along z , and we denote by L_x, L_y, L_z the unit cell dimensions (where L_z is also the electrode spacing). The particles are assumed to be charged and nonpolarizable, a good approximation for dielectric colloids, and fully screened by Debye layers of characteristic thickness $\lambda_D \ll a$. In this regime, the particles and their Debye layers

*dstn@illinois.edu

behave like insulators and their permittivity does not play a role. A voltage difference is applied between the electrodes and generates a uniform ac electric field $\mathbf{E}_0(t) = \pm E_0 \hat{\mathbf{z}}$ given by a square wave of frequency f . The field frequency is assumed to be such that $f \gg D/\lambda_D^2$ (where D is the characteristic diffusivity of the ions in the electrolyte), and $f \gg \varepsilon \zeta E_0/a\eta$ (where ζ is the particle zeta potential), so that (i) the Debye layers are assumed to remain at equilibrium, and (ii) the linear EP motion of the particles is negligible. This corresponds to high-frequency fields ($f \sim 1$ MHz), which was indeed the regime investigated in [32]. Under these assumptions, the motion of the particles results entirely from nonlinear dipolar interactions and Brownian motion.

The method of simulation is based on the calculation of pair interactions of Saintillan [13] and on the numerical algorithm described in detail in our previous work [14]. Particle positions are advanced using a Langevin equation that models the displacement of a given particle α over a time step of length Δt as a result of dipolar interactions and Brownian fluctuations as

$$\Delta \mathbf{x}_\alpha = \mathbf{v}_\alpha \Delta t + \sqrt{\frac{2k_B T \Delta t}{6\pi\eta a}} \mathbf{n}, \quad (1)$$

where \mathbf{v}_α is the deterministic particle velocity arising from particle-particle interactions, $k_B T$ is the thermal energy of the solvent, and \mathbf{n} is a random vector whose components follow a Gaussian distribution with zero mean and unit variance.

The interaction velocity \mathbf{v}_α is obtained based on a pairwise model [14] and is expressed as

$$\mathbf{v}_\alpha = \frac{\varepsilon a E_0^2}{\eta} \sum_{\beta=1}^N \mathbf{M}(\mathbf{R}_{\alpha\beta}/a) : \hat{\mathbf{z}} \hat{\mathbf{z}}, \quad (2)$$

where \mathbf{M} is a third-order dimensionless tensor capturing the interaction of particles α and β . \mathbf{M} is a function of the relative configuration of the two spheres, and more specifically of their separation vector $\mathbf{R}_{\alpha\beta} = \mathbf{x}_\beta - \mathbf{x}_\alpha$. Based on symmetries, it is possible to show that its calculation only involves three scalar functions of the dimensionless inverse separation distance $\lambda_{\alpha\beta} = 2a/|\mathbf{R}_{\alpha\beta}|$ [13] that have previously been calculated using the method of reflections and the more accurate method of twin multipole expansions. For two widely separated spheres, the method of reflections yields the following far-field expression for the tensor \mathbf{M} :

$$\mathbf{M}_{\text{FF}}(\mathbf{R}/a) = \frac{1}{12} \mathbf{T}(\mathbf{R}/a) + O(\lambda^5), \quad (3)$$

where \mathbf{T} denotes the Green's function for a potential quadrupole, and is given in index notation as

$$T_{ijk}(\mathbf{R}) = -\frac{6}{R^5} (\delta_{ij} R_k + \delta_{ik} R_j + \delta_{jk} R_i) + 30 \frac{R_i R_j R_k}{R^7}. \quad (4)$$

In the simulations, we use a periodic version of Eq. (3) that accounts for interactions of particle α with particle β inside the computational domain, as well as with all the periodic images of particle β in the x and y directions. If particles α and β become close to each other (typically when $|\mathbf{R}_{\alpha\beta}| < 4a$), the asymptotic expression Eq. (3) for the interaction tensor becomes inaccurate, and \mathbf{M}_{FF} is replaced by a near-field tensor \mathbf{M}_{NF} , which was calculated by Saintillan [13] using the method of twin multipole expansions and is accurate down

to separation distances of the order of $|\mathbf{R}_{\alpha\beta}| \approx 2.05a$. Note that the velocity \mathbf{v}_α obtained by Eq. (2) accounts for both electric and hydrodynamic interactions between particles, but does not capture long-range interactions with the electrodes. Such interactions, which may have an effect on particle dynamics in the direct vicinity of the electrodes [35], will be included in future work.

The direct calculation of the sums in Eq. (2) is computationally intensive with a complexity of $O(N^2)$ if performed directly. To accelerate the calculation of these sums, we use the fast smooth-particle-mesh Ewald algorithm previously developed by Saintillan *et al.* [33] for Stokes point force interactions, and extended to potential quadrupole interactions in our recent work [14]. This algorithm, which is based on the Ewald summation formula of Hasimoto [34], makes use of fast Fourier transforms, thereby reducing the cost of evaluating Eq. (2) to $O(N \log N)$. This allows us to simulate large systems over very long time scales, which is necessary in order to observe the pattern formation reported in the experiments of Kumar *et al.* [31] and Agarwal and Yethiraj [32], as we demonstrate in Sec. III.

Because lubrication interactions are not included in the present model, and because of the use of finite time steps, care must be taken to prevent particle overlaps. To this end, we use a contact algorithm developed in our previous work [14] that can be shown to prevent all overlaps within roundoff errors without introducing any unphysical long-range interactions, as would be the case with a soft potential. A similar algorithm is also employed to capture excluded volume interactions with the cell electrodes and prevent particles from leaving the domain.

In the following, all variables are made dimensionless using the following length, velocity, and time scales:

$$l_c = a, \quad u_c = \frac{\varepsilon a E_0^2}{\eta}, \quad t_c = \frac{\eta}{\varepsilon E_0^2}. \quad (5)$$

Upon nondimensionalization of Eq. (1), a single dimensionless parameter emerges that compares the relative magnitude of particle convection as a result of dipolar interactions and Brownian diffusion. This electric Péclet number, defined as

$$\text{Pe} = \frac{\varepsilon a^3 E_0^2}{k_B T}, \quad (6)$$

is also often referred to as the dipole strength in the electrorheological literature [24].

III. RESULTS

A. Pattern formation

We first consider the case of negligible Brownian motion ($\text{Pe} = \infty$). Figure 1 shows snapshots from a simulation at a volume fraction of $\phi = 20\%$ in a cell of thickness $L_z = 20.5$. Starting from a random distribution, the electric field is applied at $t = 0$ and quickly leads to particle chaining in the z direction. This process occurs on a fast time scale ($t \approx 200$), and is followed by a slow rearrangement of the chains in the x - y plane. Nearby chains are first observed to coalesce into sheetlike aggregates with a clear hexagonal structure [Fig. 1(c)] that had previously been observed in other simulations [15,20]. Interactions between sheets and isolated

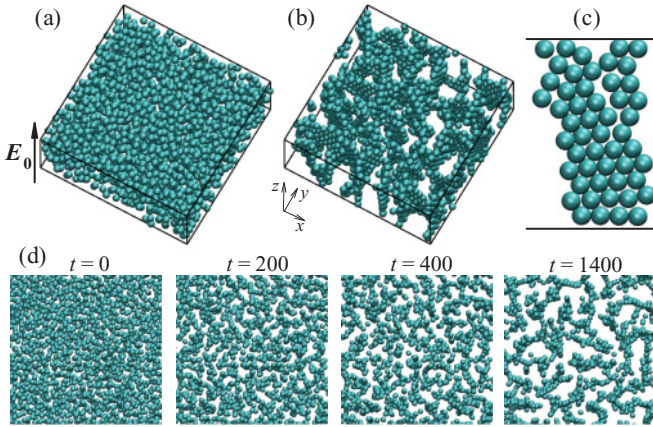


FIG. 1. (Color online) Snapshots of particle distributions in a suspension of 2000 spheres in a cell of dimensions $L_x \times L_y \times L_z = 45^2 \times 20.5$ ($Pe = \infty$, $\phi = 20\%$) at times (a) $t = 0$ (random distribution), and (b) $t = 1400$. (c) Zoom on a particle sheet in the configuration of (b). (d) Time evolution of the suspension in the x - y plane. See Ref. [36] for a movie showing the dynamics.

chains are observed to result in further sheet growth [36]. As the sheets become large enough, they connect and end up forming cellular patterns of particle-free voids surrounded by particle-rich walls [Fig. 1(d), $t = 1400$] that are reminiscent of the experimental observations [31,32]. This coarsening process is much slower than the initial chain formation. It eventually slows down, and while it is not fully clear whether an actual steady state is reached, the observed patterns do not evolve significantly after $t \approx 1000$.

We quantify the typical size of the voids in the steady-state patterns in Fig. 2. For a given particle distribution

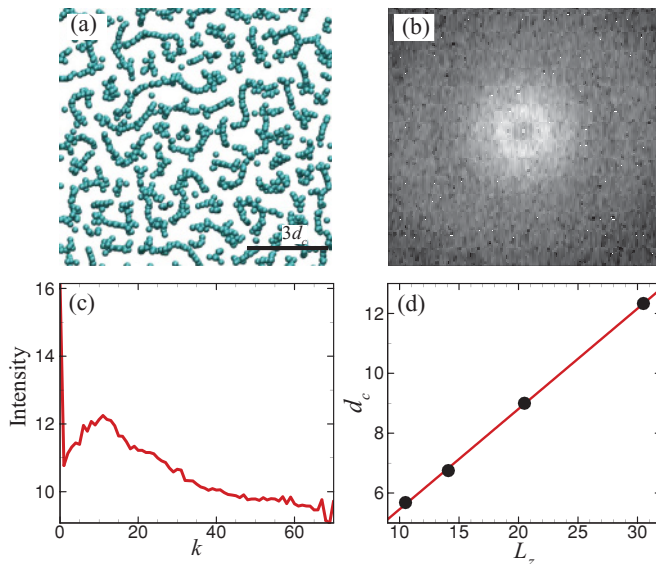


FIG. 2. (Color online) (a) Steady-state configuration in a non-Brownian suspension of 2000 spheres in a cell of dimensions $L_x \times L_y \times L_z = 62.5^2 \times 10.5$ ($Pe = \infty$, $\phi = 20\%$). (b) Two-dimensional Fourier transform of (a). (c) Circumferentially averaged intensity profile from (b). The dominant wave number corresponds to the characteristic distance d_c between structures. (d) Characteristic distance d_c as a function of electrode spacing L_z .

[Fig. 2(a)], we take a two-dimensional Fourier transform of the entire suspension in the x - y plane in Fig. 2(b). The Fourier transform exhibits a bright isotropic ring. After a circumferential averaging, the radial intensity profile shows a clear peak at a dominant wave number k that corresponds to the characteristic void size (or distance between structures) d_c in the configuration of Fig. 2(a). This process can be repeated for different electrode spacings L_z and d_c is plotted versus L_z in Fig. 2(d). The first observation is that d_c exceeds the particle dimensions by an order of magnitude. It is also found to increase almost linearly with L_z over the range of electrode spacings considered in our simulations. Both of these findings are consistent with experiments [31,32], as is the order of magnitude of d_c found here compared to experimental runs with similar geometries and volume fractions.

B. Effect of volume fraction

The effects of the volume fraction ϕ on pattern formation are analyzed in Figs. 3 and 4, where ϕ is varied from 5 to 15% for a fixed L_z and for $Pe = \infty$. As observed in Fig. 3, the steady-state morphology of the suspensions changes drastically. In very dilute suspensions, chains and sheets still form but do not connect into a cellular network as is the case at higher ϕ . This appears to differ from experiments where cellular patterns were observed even at very strong dilution ($\phi \sim 1\%$). This discrepancy may be a consequence of the small gap sizes that our simulations are limited to owing to their high computational cost.

The time dynamics and kinetics of pattern formation are illustrated more quantitatively in Fig. 4, where, following Kumar *et al.* [31], we plot the gray level $G(t)$ of the images of Fig. 4(a), which is defined as the relative brightness of the images with a range of 0 (black) to 255 (white), averaged in the x - y directions. Initially, all the curves exhibit a rapid increase in $G(t)$ owing to particle chaining in the z direction that causes

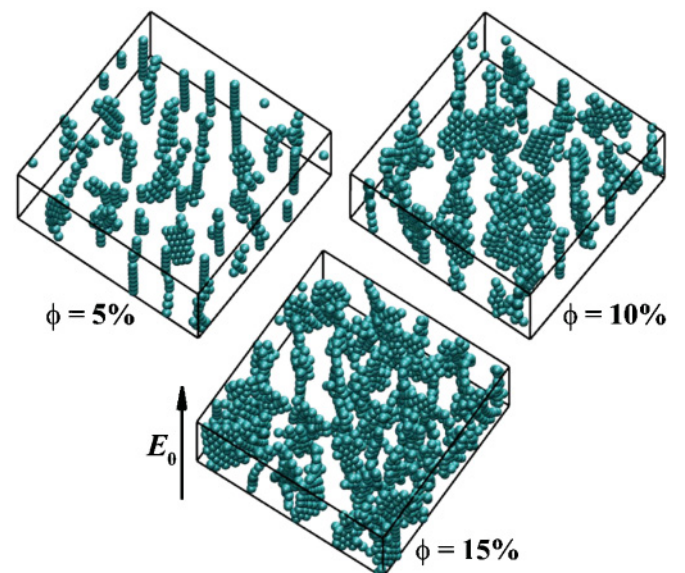


FIG. 3. (Color online) Steady-state patterns obtained in non-Brownian suspensions ($Pe = \infty$) at volume fractions $\phi = 5\%$, 10% , and 15% in a cell of dimensions $L_x \times L_y \times L_z = 45^2 \times 20.5$.

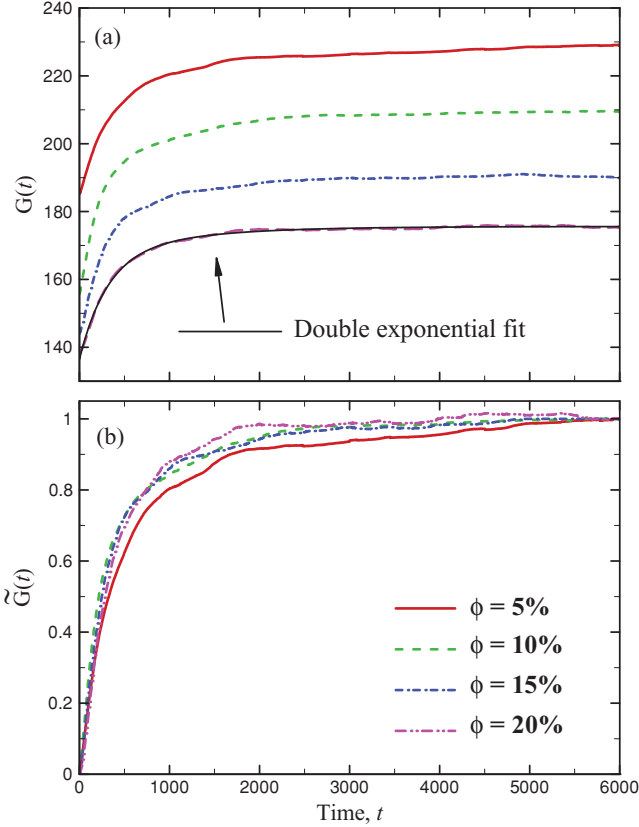


FIG. 4. (Color online) (a) Average gray level and (b) normalized gray level vs t for simulations at different volume fractions. (a) also shows a double-exponential fit in the case $\phi = 20\%$.

the formation of small voids in the images [e.g., see Fig. 1(d) at $t = 200$]. This sharp and rapid increase is then followed by a slower phase in which $G(t)$ keeps increasing slowly and eventually asymptotes. This second phase corresponds to the slow reorganization of the chains into sheets and eventually cells in the x - y plane. As expected, the average gray level is significantly larger for low ϕ but, interestingly, all the curves collapse when $G(t)$ is normalized as

$$\tilde{G}(t) = \frac{G(t) - G(t = 0)}{G(t = t_f) - G(t = 0)}. \quad (7)$$

To confirm the existence of two disparate time scales for the dynamics, we calculate a least-squares fit of the curves in Fig. 4(b) using a double exponential of the form $\tilde{G}(t) = 1 - c_1 e^{-t/\tau_1} - c_2 e^{-t/\tau_2}$, where the constants τ_1 and τ_2 ($\tau_1 < \tau_2$) should be interpreted as the characteristic time scales for chain formation and for mesoscale structure formation, respectively. Such a fit, shown in Fig. 4(a), is found to capture the time dynamics very well (residual norm ≈ 0.27) and significantly better than with a single exponential (norm ≈ 0.74). Typical values of the time constants are $\tau_1 \approx 261$ and $\tau_2 \approx 743$, which are consistent with the coarse estimates of the time scales obtained by inspection on Fig. 1. Both time scales τ_1 and τ_2 are found to increase with L_z and decrease with Pe , but do not vary significantly with ϕ .

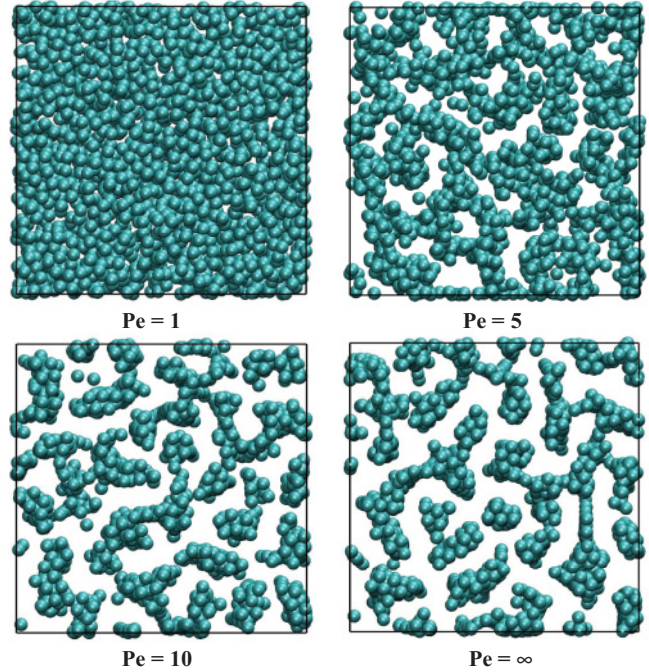


FIG. 5. (Color online) Effect of Brownian motion on pattern formation. Steady-state patterns obtained in suspensions of volume fraction $\phi = 20\%$ in a cell of dimensions $L_x \times L_y \times L_z = 45^2 \times 20.5$ at various Péclet numbers.

C. Effect of Brownian motion

The effects of Brownian motion are considered in Fig. 5, where electric field strength is varied systematically. At very low Pe ($Pe \lesssim 2$, strong Brownian motion) no clear structure formation is observed in the simulations owing to the predominance of thermal fluctuations that randomize particle configurations. As field strength increases ($Pe = 5$) voids appear in the suspensions indicating chain formation but the structure remains fairly random without any clear cellular patterns. It is instead composed of thick columnar structures (with widths of a few particle radii) that fluctuate but do not rearrange into sheets. As the Péclet number keeps increasing the structures become cleaner, with the formation of sheets and cellular patterns starting to occur beyond $Pe \approx 10$. Above $Pe \approx 100$, the effects of Brownian motion become negligible and steady-state structures become very similar to the non-Brownian case of Fig. 1. These observations are confirmed in Fig. 6, showing $G(t)$ and $\tilde{G}(t)$ for various values of Pe . Beyond $Pe = 100$, the various curves become indistinguishable.

The transition from disordered to ordered states as Pe increases is demonstrated clearly in the inset of Fig. 6(b), showing the characteristic void size d_c versus Pe . In particular, d_c exhibits a sharp transition around $Pe \approx 5$ from the low value of ≈ 2 to $3a$ to the significantly higher mesoscale value of $\approx 9a$, indicative of the onset of order and pattern formation under the action of the field. A similar increase was also reported in experiments, where the transition also occurred around $Pe \approx 5$ [32]. This disorder-order transition, in which Pe plays the role of a control parameter, suggests an easy way of adjusting the microstructure and corresponding effective

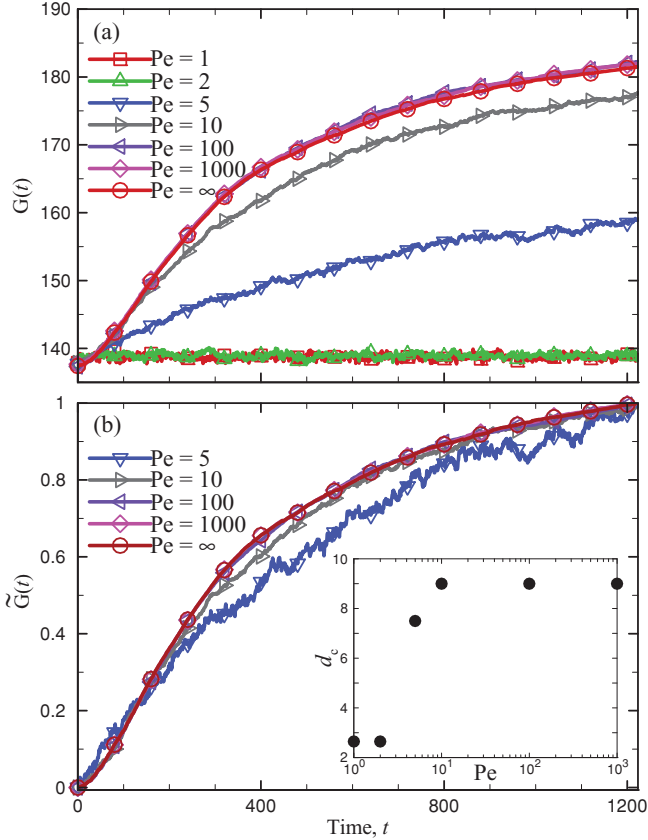


FIG. 6. (Color online) (a) Average gray level and (b) normalized gray level vs t for different values of Pe . Inset: characteristic distance d_c between structures (measured by the method of Fig. 2) vs Péclet number.

properties (e.g., optical transmittance, thermal conductivity) of colloidal suspensions in practical applications by simply tuning up the strength of the applied electric field.

D. Chain-chain interactions

Because dipolar interactions are the only driving force in our simulations, it is natural to assume that the observed pattern formation is a consequence of dipolar interactions between chains. This was already speculated by Agarwal and Yethiraj [32]. To test this hypothesis and gain insight into the wave number selection, we calculate the relative velocity between two straight finite particle chains using the same algorithm as used in the suspension simulations. The relative velocity [Fig. 7(a)] is found to be attractive in the near field but repulsive in the far field, with a transition occurring at a critical distance D_c , which is a function of chain length (or L_z). The dependence of D_c on L_z is shown in Fig. 7(b) and follows a power law with exponent ≈ 0.50 . While this dependence differs from the linear law obtained in Fig. 2(d) for the characteristic distance d_c between structures, replotting both sets of data together in the inset of Fig. 7(b) shows that the increase in D_c with L_z is also well captured by a linear law over the range of electrode spacings considered in the simulations. We also note a direct correspondence between d_c and D_c over this range, with an approximate law given by $d_c \approx 2D_c$. This strongly suggests that the size of the cellular patterns is controlled by the balance

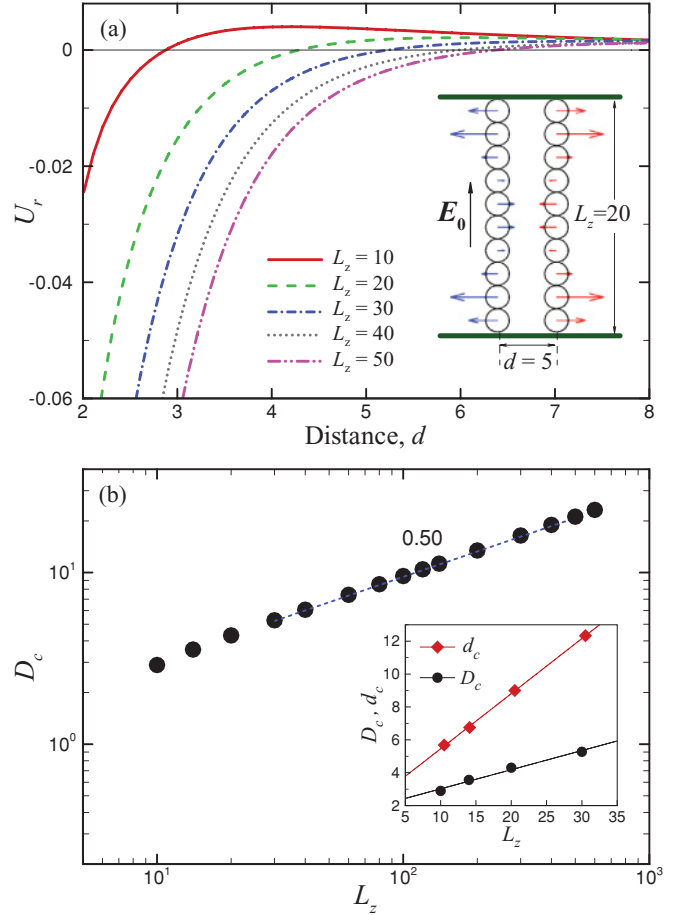


FIG. 7. (Color online) (a) Relative velocity U_r between two straight and parallel chains of length L_z vs distance d between the chains. Inset: geometry of the two chains in the case $L_z = 20$, where the arrows show the individual particle velocities. (b) Critical distance D_c at which $U_r = 0$ as a function of chain length L_z . Inset: characteristic distance d_c between structures [from Fig. 2(d)] and critical distance D_c [from Fig. 5(b)] over the range $L_z = 10$ –30.

between near-field attraction and far-field repulsion between chains, yielding steady-state structures with a characteristic wavelength of the order of the equilibrium distance D_c .

IV. CONCLUDING REMARKS

We have presented a computational study of the long-time structure formation occurring in colloidal sphere suspensions in an electric field using a detailed algorithm that accounts for dipolar interactions (including both near-field and far-field electric and hydrodynamic interactions), as well as Brownian motion. Using a fast smooth-particle-mesh Ewald algorithm we were able to simulate large systems efficiently, which allowed us to probe long-time scales. We found in our simulations that the rapid chain formation that takes place initially as a result of dipolar interactions is followed by a slow coarsening process, characterized by the formation of hexagonal sheets, that eventually leads to mesoscale cell patterns, in good agreement with experiments [31,32]. This coarsening process was shown to be a result of interactions between chains. While the precise physical mechanism for

this coarsening and for the wave number selection is not fully understood, our simulations suggest that the pattern formation observed in the suspensions may be determined by the balance between near-field attraction and far-field repulsion between particle chains. Most interestingly, our simulations demonstrate that the suspension's volume fraction, electrode spacing, and field strength all have a significant impact on the morphology and characteristic size of the rich structures that emerge at steady state, suggesting novel ways of controlling

and manipulating the microstructure and effective properties of colloidal suspensions in technological applications.

ACKNOWLEDGMENTS

The authors thank Andreas Acrivos and Boris Khusid for fruitful discussions and gratefully acknowledge funding from Lawrence Livermore National Laboratory under Subcontract No. DOE-B583843.

-
- [1] S.-R. Yeh, M. Seul, and B. I. Shraiman, *Nature (London)* **386**, 57 (1997).
- [2] X. G. Xiong, P. Makaram, A. Busnaina, K. Bakhtari, S. Somu, N. McGruer, and J. Park, *Appl. Phys. Lett.* **89**, 193108 (2006).
- [3] S. J. Williams, A. Kumar, and S. T. Wereley, *LOC* **8**, 1879 (2008).
- [4] X. Y. Hu, P. H. Bessette, J. R. Qian, C. D. Meinhart, P. S. Daugherty, and H. T. Soh, *Proc. Natl. Acad. Sci. USA* **102**, 15757 (2005).
- [5] S. J. Williams, A. Kumar, N. G. Green, and S. T. Wereley, *J. Micromech. Microeng.* **20**, 015022 (2010).
- [6] A. E. Cohen and W. E. Moerner, *Appl. Phys. Lett.* **86**, 093109 (2005).
- [7] A. E. Cohen, *Phys. Rev. Lett.* **94**, 118102 (2005).
- [8] D. A. Saville, *Annu. Rev. Fluid Mech.* **9**, 321 (1977).
- [9] H. A. Pohl, *Dielectrophoresis* (Cambridge University Press, Cambridge, England, 1978).
- [10] J. Kadaksham, P. Singh, and N. Aubry, *Mech. Res. Commun.* **33**, 108 (2006).
- [11] A. A. Füredi and R. C. Valentine, *Biochim. Biophys. Acta* **56**, 33 (1962).
- [12] T. B. Jones, *Electromechanics of Particles* (Cambridge University Press, Cambridge, England, 1995).
- [13] D. Saintillan, *Phys. Fluids* **20**, 067104 (2008).
- [14] J. S. Park and D. Saintillan, *J. Fluid Mech.* **662**, 66 (2010).
- [15] T. C. Halsey and W. Toor, *Phys. Rev. Lett.* **65**, 2820 (1990).
- [16] T. C. Halsey and W. Toor, *J. Stat. Phys.* **61**, 1257 (1990).
- [17] J. E. Martin, J. Odinek, and T. C. Halsey, *Phys. Rev. Lett.* **69**, 1524 (1992).
- [18] M. Gross and S. Kiskamp, *Phys. Rev. Lett.* **79**, 2566 (1997).
- [19] E. M. Furst and A. P. Gast, *Phys. Rev. E* **62**, 6916 (2000).
- [20] J. E. Martin, R. A. Anderson, and C. P. Tigges, *J. Chem. Phys.* **108**, 3765 (1998).
- [21] U. Dessanayake, S. Fraden, and A. van Blaaderen, *J. Chem. Phys.* **112**, 3851 (2000).
- [22] B. Khusid and A. Acrivos, *Phys. Rev. E* **60**, 3015 (1999).
- [23] P. M. Adriani and A. P. Gast, *Phys. Fluids* **31**, 2757 (1988).
- [24] A. P. Gast and C. F. Zukoski, *Adv. Colloid Interface Sci.* **30**, 153 (1989).
- [25] T. C. Halsey, *Science* **258**, 761 (1992).
- [26] M. Parthasarathy and D. J. Klingenberg, *Mater. Sci. Eng. Rep.* **R17**, 57 (1996).
- [27] P. J. Rankin, J. M. Ginder, and D. J. Klingenberg, *Curr. Opin. Colloid Interface Sci.* **3**, 373 (1998).
- [28] K. von Pfeil, M. D. Graham, D. J. Klingenberg, and J. F. Morris, *Phys. Rev. Lett.* **88**, 188301 (2002).
- [29] R. Haghgooie and P. S. Doyle, *Phys. Rev. E* **72**, 011405 (2005).
- [30] R. Haghgooie and P. S. Doyle, *Phys. Rev. E* **75**, 061406 (2007).
- [31] A. Kumar, B. Khusid, Z. Y. Qiu, and A. Acrivos, *Phys. Rev. Lett.* **95**, 258301 (2005).
- [32] A. K. Agarwal and A. Yethiraj, *Phys. Rev. Lett.* **102**, 198301 (2009).
- [33] D. Saintillan, E. Darve, and E. S. G. Shaqfeh, *Phys. Fluids* **17**, 033301 (2005).
- [34] H. Hasimoto, *J. Fluid Mech.* **5**, 317 (1959).
- [35] W. D. Ristenpart, I. A. Aksay, and D. A. Saville, *J. Fluid Mech.* **575**, 83 (2007).
- [36] See supplemental material at [<http://link.aps.org/supplemental/10.1103/PhysRevE.83.041409>] [for two supplementary movies].